Probing H_2 autoionizing states with femto- and attosecond laser pulses

2009 J. Phys.: Conf. Ser. 194 012013

(http://iopscience.iop.org/1742-6596/194/1/012013)

Journal of Physics: Conference Series **194** (2009) 012013 doi:10.1088/1742-6596/194/1/012013

Probing H_2 autoionizing states with femto- and attosecond laser pulses.

J L Sanz-Vicario[1], J F Pérez-Torres[2], F Morales[2], E Plessiat[2] and F Martín[2]

[1] Grupo de Física Atómica y Molecular, Instituto de Física, Universidad de Antioquia, AA1226 Medellín, Colombia

[2] Departamento de Química C-9, Universidad Autónoma de Madrid, 28049 Madrid, Spain

E-mail: sanjose@fisica.udea.edu.co

Abstract.

We show the relevance that molecular autoionizing states display in some recent experiments related to the symmetry-breaking in molecular-frame photoelectron angular distributions in H_2 when exposed to intense xuv femtosecond laser pulses, and others related to the electron (proton) localization when subject to attosecond pump-probe laser schemes. Our theoretical method solves the time-dependent Schrödinger equation with an spectral method that expands the wave function in terms of H_2 correlated stationary vibronic states including all electronic and vibrational degrees of motion. Time-resolved asymmetric electron angular distributions are obtained at specific proton kinetic energies due to the delayed autoionization from H_2 doubly excited states, which induces interferences between *gerade* ($1s\sigma_g$) and *ungerade* ($2p\sigma_u$) ionization channels. We also study photoionization of H_2 exposed to a xuv attosecond pump pulse plus a time-delayed IR femtosecond probe pulse. Fast alternating asymmetries in the proton ejection (electron localization) are obtained as a function of the time delay between the pump and the probe pulses. Finally, we deal with the process of (xuv) two-photon double ionization of H_2 under the assumption of having both sequential and non-sequential absorption processes.

1. Introduction

Ultrashort femto (fs) and attosecond (as) laser pulses in the xuv region and tunable intensities up to 10^{14} W/cm^2 are currently generated through high-order harmonic generation (HHG) and progressively available from free electron lasers (FEL) at even higher intensities. Also, time-delayed radiation pulses in pump-probe schemes, presently generated by these sources, enable the prospect of time-resolved spectroscopy to keep track of fast electronic and nuclear motions in small molecules at attosecond time scales. Attosecond xuv pulses have already been applied to verify the exponential Auger decay of core-excited states in atoms [1], which would allow the possibility of investigating the complex non-exponential decay of molecular autoionizing states and the ensuing expected effects in experimental observables, namely, angular and kinetic energy distributions of fragments after dissociative photoionization. Furthermore, attosecond pulse technology may be combined in the next future with kinematically complete experiments, in which the momentum of all ejected fragments (electrons and ions) is determined in coincidence. Such an experimental scenario may provide unprecedented insight into the dynamics of molecular photoionization, provided that theoretical developments also meet the accompanying challenges.

To answer some of the emergent questions, we have developed a sophisticated time-dependent method to study photoionization processes in H_2 when exposed to isolated xuv fs laser pulses as well as time-delayed pump-probe xuv(as)-IR(fs) lasers. In the former case, we are able to obtain time-resolved molecular-frame photoelectron angular distributions to better understand the symmetry-breaking with respect to the nuclei inversion [2]. In the latter case, asymmetries in the direction of proton ejection (or, equivalently, in the electron localization) are obtained as a function of the time delay (with attosecond resolution) between a xuv 400 as pump and an IR 16 fs probe. Our results are supported by a recent attosecond molecular experiment [3]. Finally, other recent experiments [4] for two-photon double ionization of D_2 at photon energies of 38 eV can be also understood in terms of a pump-probe scheme of two identical photons absorbed either instantaneously with zero delay (direct nonsequential process) or after a given time delay (sequential process). We propose here a very simple theoretical model to interpret the peaks appearing in the kinetic energy of photodissociation fragments.

2. Theoretical Method

In order to resolve the dynamics of the hydrogen molecule subject to ultrashort laser pulses in the time domain, we use an spectral method for the solution of the time-dependent Schrödinger equation (TDSE), that reads (atomic units are used unless otherwise stated)

$$\left(\mathcal{H}^{(0)}(\mathbf{r},R)+V(t)-i\frac{\partial}{\partial t}\right)\Phi(\mathbf{r},R,t)=0, \tag{1}$$

where $\mathbf{r}$ labels both electronic coordinates $\mathbf{r}_1$ and $\mathbf{r}_2$, R is the internuclear distance and $\mathcal{H}^{(0)}$ is the H_2 field-free non-relativistic Hamiltonian, $\mathcal{H}^{(0)}=-\nabla_R^2/2\mu+\mathcal{H}_{el}(\mathbf{r},R)$. Here $\mathcal{H}_{el}$ is the electronic Hamiltonian (including the $1/R$ repulsion term) and $V(t)=\mathbf{p}\cdot\mathbf{A}(t)$ represents the laser-molecule interaction potential in the semiclassical dipole approximation, where $\mathbf{p}$ is the dipole operator and $\mathbf{A}(t)$ is the vector potential. The latter corresponds to a pulse with a photon energy ω and duration T, linearly polarized parallel to the internuclear axis (selection rule $\Delta\Lambda$=0 applies) or perpendicular to it ($\Delta\Lambda=\pm1$). Its modulus for $t\in[0,T]$ is

$$A(t)=A_0\sin^2\left(\frac{\pi t}{T}\right)\cos\omega t \tag{2}$$

and zero elsewhere, and the laser intensity I is related to the vector potential amplitude A_0 through $I=A_0^2\omega^2$. In our spectral method [5, 6], the total time-dependent wave function $\Phi(\mathbf{r},R,t)$ is expanded in a basis of fully correlated adiabatic Born-Oppenheimer (BO) vibronic stationary states of energy W_k, which include the bound states, the doubly excited states and the non resonant continuum states of H_2:

$$\begin{aligned}\Phi(\mathbf{r},R,t) &= \sum_n \sum\!\!\!\!\!\!\int_{v_n} C_{nv_n}(t)\phi_n(\mathbf{r},R)\chi_{v_n}(R)e^{-iW_{nv_n}t}+\sum_r \sum\!\!\!\!\!\!\int_{v_r} C_{rv_r}(t)\phi_r(\mathbf{r},R)\chi_{v_r}(R)e^{-iW_{rv_r}t}\\ &+ \sum_{\alpha,\ell_\alpha}\int d\varepsilon_\alpha \sum\!\!\!\!\!\!\int_{v_\alpha} C^{\ell_\alpha\varepsilon_\alpha}_{\alpha v_\alpha}(t)\psi^{\ell_\alpha\varepsilon_\alpha}_\alpha(\mathbf{r},R)\chi_{v_\alpha}(R)e^{-iW_{\varepsilon_\alpha v_\alpha}t}\end{aligned} \tag{3}$$

where ϕ_n, ϕ_r and $\psi_\alpha^{\ell\varepsilon}$ represent the bound, doubly excited and continuum electronic states of H_2, respectively (see figure 1). Here, α denotes the full set of quantum numbers for the electronic state of the residual molecular ion H_2^+ with BO energy $E_\alpha(R)$ and the indices ℓ_α and ϵ_α correspond, respectively, to the angular momentum and the kinetic energy of the ejected electron in channel α. The electronic states in Eq. (3) result from the solution of the following eigenvalue equations: i)$[\mathcal{H}_{el}-\mathcal{E}_n(R)]\,\phi_n(\mathbf{r},R)=0$, ii)$[\mathcal{Q}\mathcal{H}_{el}\mathcal{Q}-\mathcal{E}_r(R)]\,\phi_r(\mathbf{r},R)=0$ and iii) $[\mathcal{P}\mathcal{H}_{el}\mathcal{P}-\mathcal{E}_\alpha^{\varepsilon_\alpha}(R)]\,\psi_\alpha^{\ell_\alpha\varepsilon_\alpha}(\mathbf{r},R)=0$, where $\mathcal{P}$ and $\mathcal{Q}=1-\mathcal{P}$ are Feshbach projection operators

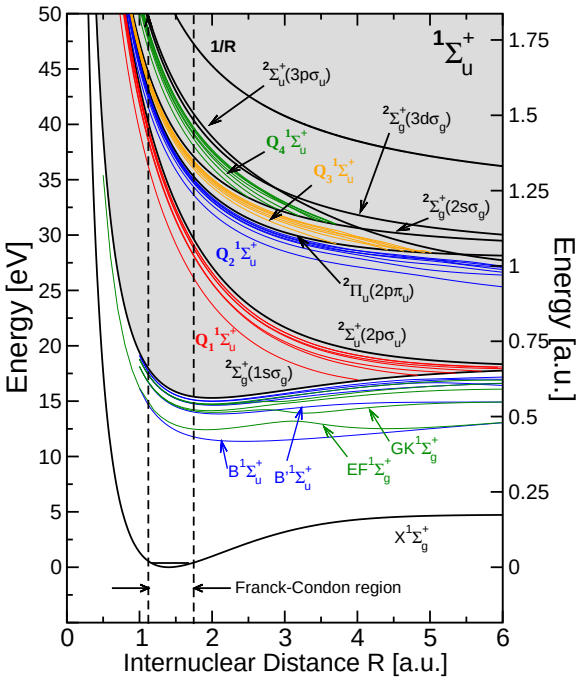

Figure 1. (color online) Potential energy curves of H_2. The figure shows the six lowest singly excited states of $^1\Sigma_u^+$ and $^1\Sigma_g^+$ symmetry below the first H_2^+ threshold. Above the latter (within the shadowed area) the Q_1, Q_2, Q_3 and Q_4 doubly excited states of H_2 of $^1\Sigma_u^+$ symmetry are displayed below their corresponding H_2^+ thresholds (also indicated with arrows).

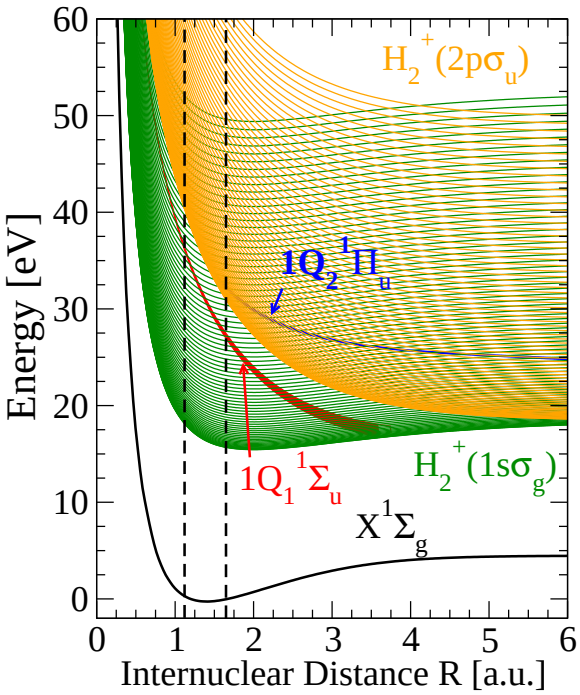

Figure 2. (color online) Discretized basis of continuum electronic states included in this work corresponding to the H_2^+ $(1s\sigma_g)$ and H_2^+ $(2p\sigma_u)$ ionization thresholds. As example, the lowest $\mathcal{Q}_1$ $^1\Sigma_u^+$ and $\mathcal{Q}_2$ $^1\Pi_u$ autoionizing states are embedded in the continuum and the line thickness for these dissociative resonances corresponds to the energy broadening due to their respective autoionizing widths.

that project onto the resonant and non resonant parts of the continuum wave function and the electronic continuum states have an energy $\mathcal{E}_\alpha^{\varepsilon_\alpha}(R) = E_\alpha(R) + \varepsilon_\alpha$ (see figure 2). The vibrational (bound and dissociative) wave functions χ_{v_n}, χ_{v_r} and χ_{v_α} are the solutions of a one-dimensional Schrödinger equation that represents the relative motion of the two nuclei in the presence of the potentials $\mathcal{E}_n(R)$, $\mathcal{E}_r(R)$ and $\mathcal{E}_\alpha^{\varepsilon_\alpha}(R)$, respectively. For the electronic calculations of bound and resonant states we make use of a CI procedure using H_2^+ orbitals, represented in terms of a basis set of 180 B-splines of order k=8, including angular momenta from ℓ=0 to ℓ=16 within a radial box of size 60 a.u. Wave functions for the non resonant continuum $\psi_\alpha^{\ell\varepsilon}$ are computed using a $\mathcal{L}^2$ close-coupling approach following the procedure in Ref. [7]. By introducing the ansatz (3) in the TDSE (1) one arrives to a set of coupled differential equations, which are integrated in time beyond the pulse duration T (and also beyond the lifetime of resonant states to let them decay) in order to get the expansion coefficients $C_i(t \to \infty)$, which are the basic quantities to extract (by projecting appropriately) any dissociative photoionization probability. Besides, $\psi_\alpha^{\ell_\alpha\varepsilon_\alpha}(\mathbf{r}, R)$ states are indeed eigenstates of the unperturbed field-free Hamiltonian, and the projection of the total wave function $\Phi(\mathbf{r}, R, t)$ onto the $\psi_\alpha^{\ell_\alpha\varepsilon_\alpha}(\mathbf{r}, R)$ states at $t > T$ leads to probability amplitudes that can be correctly expressed in terms of the $C_{\alpha v_\alpha}^{\ell_\alpha\varepsilon_\alpha}$ expansion coefficients.

In particular, in experiments using multicoincidence reaction microscopes in which the momentum of all emitted fragments (electrons and protons) is detected simultaneously, the

direction in which the proton escapes along the internuclear axis in a dissociative ionization process $H_2+\omega \rightarrow H^+ + H + e^-$ can be elucidated. Thus, molecular frame photoelectron angular distributions (MFPAD) associated to the H + H^+ and H^+ + H dissociative ionization channels may be obtained and distinguished, which means that such experiments provide a boundary condition for proton localization. To satisfy such condition the total wave function $\Phi(\mathbf{r}, R, t)$ should be projected onto stationary continuum states that localize one of the protons in a given center, for instance, up (U) or down (D), i.e., the bound electron is described asymptotically by linear combinations of H_2^+ ionization channels α. At the photon energies here considered (33 eV) the ionization channels involved are $\alpha = 1s\sigma_g, 2p\sigma_u$ and one of the electrons (namely, electron 1) is described by the localized wave function $1s_{U,D}(\mathbf{r}_1) = \frac{1}{\sqrt{2}}[1s\sigma_g(\mathbf{r}_1) \pm 2p\sigma_u(\mathbf{r}_1)]$. Accordingly, the partial wave form of the asymptotically localized continuum state reads

$$\Phi_{U,D} = \frac{1}{\sqrt{2}} \sum_{\ell,m} i^\ell e^{-i\sigma_\ell(\varepsilon)} \mathcal{Y}^*_{lm}(\Omega_e) \left[\psi^{\ell\varepsilon}_{1s\sigma_g} \chi_{v_g} e^{-iW_{1s\sigma_g,v_g}t} \pm \psi^{\ell\varepsilon}_{2p\sigma_u} \chi_{v_u} e^{-iW_{2p\sigma_u,v_u}t} \right], \tag{4}$$

where $\sigma_\ell(\varepsilon) = arg\Gamma(\ell + 1 - i/\sqrt{2\varepsilon})$ is the Coulomb phase shift. Here and hereafter the electron angular momentum value ℓ in the sums must be compatible with the total *gerade* ($^1\Sigma_g^+$) or *ungerade* ($^1\Sigma_u^+$) symmetry of the two-electron state. In one-photon excitation only the final $^1\Sigma_u^+$ continuum states for each H_2^+ ionization channel are reached, but in multiphoton pump-probe lasers both $^1\Sigma_g^+$ and $^1\Sigma_u^+$ states are populated. By projecting the total time dependent wave packet $\Phi(\mathbf{r}, R, t)$ onto the latter U or D asymptotic state one obtains the following expression for the ionization probability, differential in both proton kinetic energy and solid angle of the ionized electron:

$$\frac{d^2P_{U,D}}{dE_{H^+}d\Omega_e} = \frac{1}{2} \int d\varepsilon \left| \sum_{\ell,m} i^{-\ell} e^{i\sigma_\ell(\varepsilon)} \mathcal{Y}_{lm}(\Omega_e) (C^{\ell\varepsilon}_{1s\sigma_g v_g} \pm C^{\ell\varepsilon}_{2p\sigma_u v_u}) \right|^2. \tag{5}$$

Now, integrating over the solid angle, we may also obtain kinetic energy distributions for protons measured in the up or down direction

$$\frac{dP_{U,D}}{dE_{H^+}} = \frac{1}{2} \int d\varepsilon \sum_\ell \left(|C^{\ell\varepsilon}_{1s\sigma_g v_g}|^2 \pm 2Re(C^{\ell\varepsilon *}_{1s\sigma_g v_g} C^{\ell\varepsilon}_{2p\sigma_u v_u}) + |C^{\ell\varepsilon}_{2p\sigma_u v_u}|^2 \right), \tag{6}$$

and the total kinetic energy spectrum of protons (up + down) thus is

$$\frac{dP}{dE_{H^+}} = \int d\varepsilon \sum_\ell \left(|C^{\ell\varepsilon}_{1s\sigma_g v_g}|^2 + |C^{\ell\varepsilon}_{2p\sigma_u v_u}|^2 \right). \tag{7}$$

In order to connect with experiments which may detect protons in both directions (up or down), we define the nuclear asymmetry parameter β as follows:

$$\beta(E_{H^+}) = \left(\frac{dP_U}{dE_{H^+}} - \frac{dP_D}{dE_{H^+}} \right) / \frac{dP}{dE_{H^+}}. \tag{8}$$

Similarly, we define the asymmetry parameter for electron ejection by integrating in Eq. (5) the electron angular coordinates $d\Omega_e$ only in the upper or in the lower semisphere.

3. Results

3.1. Molecular-frame electron angular distributions.

The combination of xuv laser pulses with multicoincidence detection techniques paved the way to obtain fully differential photoelectron angular distributions for specific fragment (electrons

and protons) energies and for well defined molecular orientations with respect to the laser polarization axis. Recently, MFPAD were observed to break the inversion symmetry of H_2 for linearly polarized synchrotron radiation of 33 eV and molecules oriented perpendicular to the polarization axis. This asymmetry was theoretically attributed to the efficient interference between ionization channels of different inversion symmetry, $1s\sigma_g$ and $2p\sigma_u$, mediated by the delayed autoionization process from $\mathcal{Q}_2\ ^1\Pi_u$ doubly excited states [2]. This theoretical prediction was obtained within the framework of stationary scattering theory assuming radiation pulses of infinite duration [8]. Here we investigate the origin of the asymmetry by using instead a time-dependent method [9], that allows us to visualize the evolution of the photoelectron angular distributions in time and its interplay with the autoionization process. We include in figure 3 the ionization probability as a function of the proton kinetic energy release (KER) for a pulse of 33 eV, intensity I=10^{12} W/cm^2 and pulse duration T=10 fs. In the present case, H_2 is oriented parallel to the polarization axis and protons are emitted along this direction. This amounts to consider only transitions among the Σ molecular states.

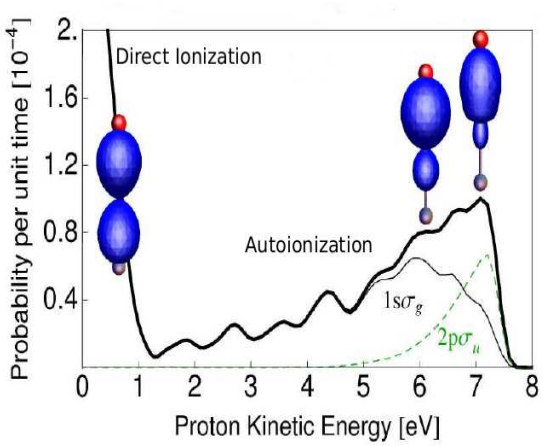

Figure 3. (color online) Proton kinetic energy spectrum and molecular frame photoelectron angular distributions for H_2 subject to a xuv laser pulse of ω=33 eV, intensity I=10^{12} W/cm^2 and duration T=10 fs for polarization parallel to the molecular axis. Thick solid line: total ionization probability; thin solid line: contribution from the $1s\sigma_g$ ionization channel; thin dashed line: contribution from the $2p\sigma_u$ ionization channel. Electron angular distributions in display correspond to proton kinetic energies 0.6, 6.1 and 7.1 eV. The molecular axis is oriented vertically and H^+ and H are indicated, respectively, by red (upper) and grey (lower) balls.

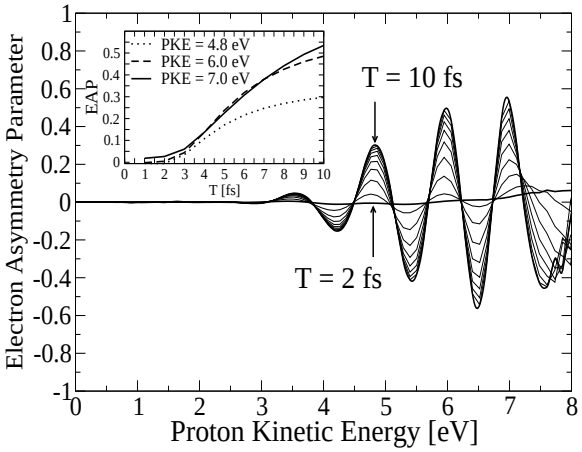

Figure 4. Asymmetry in the H_2 photoelectron angular distribution vs. proton kinetic energy for an assortment of pulses with photon energy 33 eV, intensity I=10^{12} W/cm^2 and different durations from T=2 fs up to T=10 fs. The inset shows the behaviour of the electron asymmetry with pulse duration for three different KERs (4.8, 6.0 and 7.0 eV) for which asymmetry presents a maximum and electrons move preferably in the proton direction (up). This figure explains the symmetry in the electron angular distributions at proton kinetic energy 0.6 eV, and the asymmetry (most of electron ejection upwards) for 6.1 and 7.1 eV in figure 3.

In order to explicitly show the correlation between nuclear and electronic motion, we also include MFPADs obtained at $T > 10$ fs at three specific proton energies. Electron asymmetry is absent in the region of direct ionization to the $1s\sigma_g$ continuum (low KER), and it is evident in the region where, firstly, autoionization from the $\mathcal{Q}_1$ resonances into the $1s\sigma_g$ continuum channel enhances ionization at higher KER and, secondly, there is a significant overlap between

the $1s\sigma_g$ and $2p\sigma_u$ ionization channels. This overlap is present only if autoionization from $\mathcal{Q}_1$ doubly excited states is included in the calculation, and angular asymmetries start to develop as early as $t \sim 2$ fs, approximately the autoionization lifetime of the lowest $\mathcal{Q}_1$ $^1\Sigma_u$ resonant state. To supplement this finding, figure 4 shows the electron asymmetry parameter (see Theory section) versus KER for a set of pulses of different duration (T=2-10 fs). Ultrashort pulses with duration $T \leq 2$ fs preclude electron asymmetry, since there is no time enough to develop *gerade-ungerade* interferences. The pattern of oscillations in figure 4 reflects the particular quantum interference between the two H_2 $^1\Sigma_u^+$ ionization continua, which is quite robust against different pulse durations. This oscillatory pattern in the parallel orientation case implies that even in the region where autoionization dominates symmetric angular distributions are expected at those specific KER where nodes are present, at variance with the perpendicular orientation case (not shown) in which asymmetry always happens.

3.2. H_2 exposed to attosecond pump-probe laser pulses.

Following closely a pump-probe scheme used in a recent experiment [3], we expose the H_2 molecule to the combined effect of an attosecond xuv pulse (with photon energy ω_{xuv}=30 eV, duration T_{xuv}=400 as and intensity I_{xuv}=10^9 W/cm^2) and a femtosecond few-cycle IR pulse (with photon energy ω_{IR}=1.65 eV, duration T_{IR}=16 fs and intensity I_{IR}=$3 \cdot 10^{12}$ W/cm^2) separated by a peak-peak time delay τ, which is varied from -5 to +12 fs. Large positive delays imply that the IR pulse acts much later than xuv excitation. We assume that both lasers have polarization parallel to the molecular axis. The theoretical implementation of this pump-probe scheme makes our method very demanding computationally. In spite of the symmetry restriction to Σ states due to the selected molecular orientation, we must include $^1\Sigma_g^+$ and $^1\Sigma_u^+$ continuum states associated with both $H_2^+(1s\sigma_g)$ and $H_2^+(2p\sigma_u)$ ionization channels because IR photons induce $g-u$ transitions among these continua. Thus molecular continuum-continuum dipolar couplings have been computed and included in the interaction matrix. Furthermore, due to the broad bandwidth of the xuv as pulse ($\sim$ 20 eV) all continuum states (and their vibrational ones) below 50 eV (see figure 2) were included in the calculation, in addition to bound states and the lowest $\mathcal{Q}_1$ and $\mathcal{Q}_2$ doubly excited states. It results in large scale close-coupling computations in terms of more than 100,000 vibronic states.

Figure 5 shows calculated proton KER distributions as a function of the relative xuv-IR time delay. In the region where both pulses overlap ($\tau \sim 0$ fs) one observes a significant increase of the ionization yield for high energy protons at $\sim$ 6-8 eV along with a decrease at intermediate kinetic energies, 3-5 eV (see also figure 3 for reference). This increase can be explained in terms of i) an enhancement of the ionization into the $2p\sigma_u$ channel due to IR-laser $^1\Sigma_g - ^1\Sigma_u$ mixing from $1s\sigma_g$ and $2p\sigma_u$ ionization channels. ii) IR-photoionization of initially populated $\mathcal{Q}_1$ resonances. For larger time delays ($\tau > 5$ fs), autoionization is almost complete and these contributions at 6-8 eV eventually dissappear. The most noticeable feature appears at low kinetic energies (< 2 eV) and larger time delays ($\tau > 5$ fs), which is attributed to bond softening of the bound H_2^+ $^2\Sigma_g^+$ $(1s\sigma_g)$ vibrational wave packet induced by IR photons. In fact, its maximum is located at $\tau \sim +10$ fs, just the arrival time to reach the outer turning point in the H_2^+ potential curve. In figure 6 we plot the nuclear asymmetry parameter β as a function of the delay, which provides a measure of the electron localization by detecting the direction of proton emission (up or down) with attosecond resolution. One observes strong asymmetries (U-D-U-...) that oscillate with approximately the period of the IR pulse. The asymmetry is not present when using isolated xuv pulses and is entirely caused by the presence of the IR pulse that mixes Σ_g and Σ_u continuum states corresponding to different ionization channels ($1s\sigma_g$ and $2p\sigma_u$) but the same parity for the ejected electron (ℓ_g even or ℓ_u odd). Three regions in the figure 6 (indicated by 1,2 and 3 in the plot) can be distinguished showing different patterns, tentatively associated to different mechanisms represented in figure 7. In region 1 (close xuv-IR overlap) high energy protons are

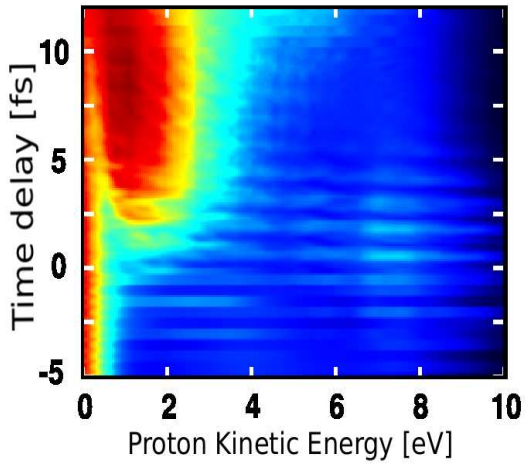

Figure 5. (color online) Proton kinetic energy distributions as a function of the time delay between the attosecond xuv pulse and the few-cycle IR pulse. Color scale follows that of Figure 6 but starting from 0 instead of -0.3 in arbitrary units.

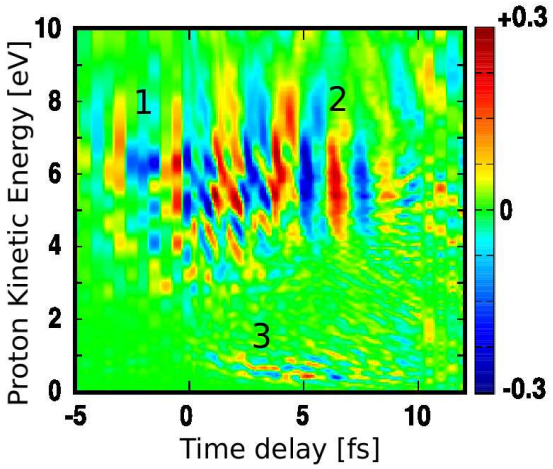

Figure 6. (color online) Proton asymmetry parameter β for the ejection of protons in xuv+IR pump-probe dissociative ionization of H_2 as a function of the proton kinetic energy release and the xuv-IR time delay. The color scheme follows the scale shown at the right side.

ejected (U or D) resulting from i) xuv excitation to ${}^1\Sigma_u^+(2p\sigma_u\varepsilon\ell_g)$ continuum, ii) then prompt IR photon absorption into ${}^1\Sigma_g^+(2p\sigma_u\varepsilon\ell_u)$ continuum before autoionization takes place and iii) a late interference with ${}^1\Sigma_u^+(1s\sigma_g\varepsilon\ell_u)$ continuum states, populated either by direct xuv ionization or mainly by delayed autoionization of the $\mathcal{Q}_1$ ${}^1\Sigma_u^+$ resonant states. Thus, autoionization at small time delays must produce a different pattern of oscillations as compared with the region of large delays. In the latter case (region 2), autoionization already elapsed and the fringes are associated to population transfer between wave packets dissociating on the $2p\sigma_u$ and $1s\sigma_g$ states of the molecular ion induced by the IR-laser. This implies that regions of large delays could be roughly described by propagating wave packets exposed to an IR-laser in a simple H_2^+ two-state model. Finally the small features in region 3 (low energy protons and large delays) are attributed to bond-softening induced by the delayed IR-pulse over the $1s\sigma_g$ states initially populated by xuv low energy photons (given the large bandwidth of the as pulse).

3.3. Two-photon double ionization: sequential versus non-sequential processes

We can also interpret recent experimental results [4] for two-photon double ionization of D_2 exposed to FEL photons of 38 eV. Measured KER distributions related to emission of two D^+ ions can be understood in terms of two additive processes: a simultaneous absorption of the two photons leading to direct double ionization and high energy ions coming from prompt Coulomb explosion, and a sequential absorption in two steps mediated by the formation of D_2^+, that yields protons at lower kinetic energy. A proper theoretical treatment for a molecular two-electron ejection combined with nuclear motion has not yet been developed. Nevertheless, we can estimate the probability for the direct (and the sequential) process assuming a simple Franck-Condon (FC) approximation. The sequential two-photon double ionization probability P_{seq}^{KER} can be obtained within our model by summing over all accessible intermediate vibrational states of the D_2^+ molecule. The probability mediated by each vibrational state v may be thus written as the product of two independent probabilities corresponding to two separated steps:

i) $D_2(v_i = 0)+\omega \rightarrow D_2^+(v)+e^-$ and ii) $D_2^+(v)+\omega \rightarrow D^+ + D^+ + e^-$, where the latter occurs after a time delay during which the nuclei evolve. Our oversimplified FC model rests in the assumption that each individual photoionization event occurs rapidly compared to vibration or dissociation so that electronic dipole matrix elements barely change with internuclear distance and they can be factored out the R-integrals. In spite of the simplicity of the model, our D^+ KER distribution is similar to the experimental findings and the physical processes involved are qualitatively explained (see Figure 8).

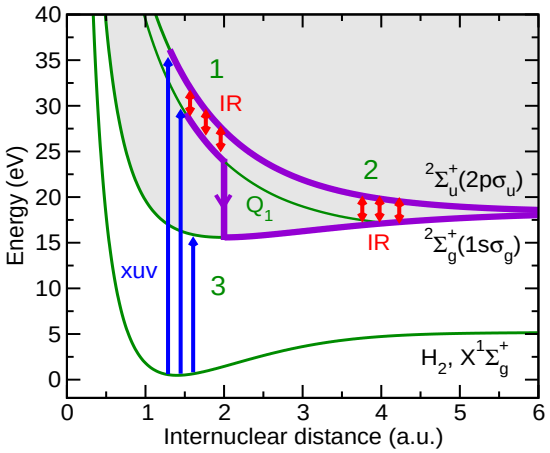

Figure 7. (color online) Three mechanisms that lead to the different proton asymmetry features in figure 6. Blue arrows indicate different photons arriving within the xuv as pulse and red arrows those of the few-cycle IR pulse; magenta lines indicate H_2 nuclear dynamics intrinsic to the molecule after photoexcitation, including the $\mathcal{Q}_1$ autoionization.

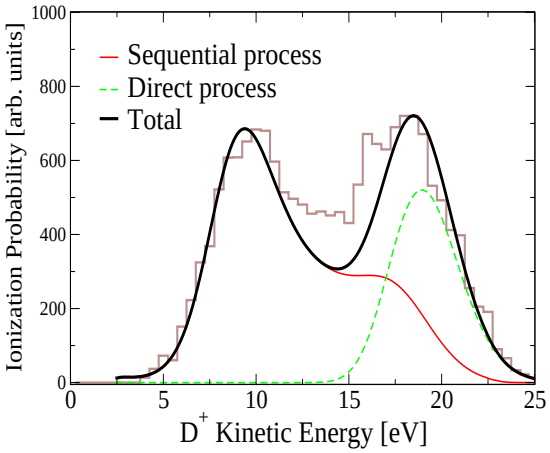

Figure 8. (color online) Two-photon double ionization probability of D_2 by a FEL pulse of 38 eV as a function of the D^+ kinetic energy release. (Black) thick solid line: total two-photon double ionization; (red) solid line: contribution from the sequential process; (green) dashed line: contribution from the direct process, and the histogram corresponds to experimental results [4].

Acknowledgments

We thank Mare Nostrum BSC and CCC-UAM for generous allocation of computer time. Work partially supported by the DGI project Nos. FIS2007-60064 and CSD2007-00010, European COST Action CM0702, Convenio Marco between Universidad de Antioquia (UdeA) and Universidad Autónoma de Madrid (UAM), J.L. S-V thanks additional financial support from Universidad de Antioquia, Colciencias agency and ICPEAC Conference, and J.F. P-T the Alban Program for Latin-America, scholarship no. E07D401391CO.

References

[1] Drescher M *et al* 2002 *Nature (London)* **419** 803
[2] Martín F *et al* 2007 *Science* **315** 629
[3] Sansone G *et al* 2009 *submitted to Nature (London)*
[4] Jiang Y H, Moshammer R and Ullrich J 2009 *private communication*
[5] Sanz-Vicario J L, Bachau H and Martín F 2006 *Phys. Rev.* A **73** 033410
[6] Sanz-Vicario J L *et al* 2007 *J. Elec. Spec. Rel. Phenom.* **161** 182
[7] Martín F 1999 *J. Phys. B: At. Mol. Opt. Phys.* **32** R197
[8] Fernández J and Martín F 2009 *New J. Phys.* **11** 043020
[9] Pérez-Torres J F, Morales F, Sanz-Vicario J L and Martín F 2009 *Phys. Rev.* A (R) **80** 011402